PERGAMON

International Journal of Solids and Structures 39 (2002) 6191–6210

INTERNATIONAL JOURNAL OF SOLIDS and STRUCTURES

www.elsevier.com/locate/ijsolstr

Stability of columns with no tension strength and bounded compressive strength and deformability. Part I: large eccentricity

Anna De Falco [a], Massimiliano Lucchesi [b,*]

[a] *Dipartimento di Ingegneria Civile, Università di Pisa, via Diotisalvi 2, Pisa 56100, Italy*
[b] *Dipartimento di Costruzioni, Università di Firenze Piazza Brunelleschi 6, Firenze 50121, Italy*

Received 31 July 2001; received in revised form 15 July 2002

Abstract

This work concerns the stability of piles with rectangular cross section, made of a no-tension material with limited compressive strength and deformability, subjected to an axial load acting within the cross section but outside its middle third (large eccentricity). The differential equations obtained have been solved explicitly, and their solutions have allowed us to describe the stability characteristics of the pile through graphical representations.

Keywords: Stability; Masonry columns; No-tension material

1. Introduction

The stability of masonry piles subjected to eccentric axial loads is a matter of a good deal of importance to applications, though in practice the slenderness involved is apparently very modest. This fact is due to the non-linear behaviour of the material, which is assumed to exhibit zero tensile strength, bounded compressive strength and deformability, and values of elastic moduli very much lower than those of concrete.

The load eccentricity may cause lateral deflection of the pile and a consequent increase in the bending moment. Cracking of the load-bearing sections may then induce a gradual reduction of the bending stiffness of the structure, until failure ensues. Such a mechanism may be triggered by either progressive instability, or because the material's limit strain has been exceeded, both of which situations would be induced by the growing deflection of the beam.

The problem is a particularly complex one because of the inherent geometric and constitutive non-linearities and, to date, has been solved analytically only by resorting to extreme simplifications. The

* Corresponding author. Tel.: +390-55-2757895; fax: +390-55-212083.
E-mail addresses: a.defalco@ing.unipi.it (A. De Falco), massimiliano.lucchesi@unifi.it (M. Lucchesi).

0020-7683/02/$ - see front matter
PII: S0020-7683(02)00467-5

earliest studies, dating back to the 1940s, treated masonry as a no-tension material with non-linear response and infinite compressive strength, and represented the beam-column through a one-dimensional model under the assumption that its cross section remains plane and orthogonal to the axis of the bent pile (see Angervo, 1954; Chapman and Slatford, 1957; Frisch-Fay, 1975, 1981; Sahlin, 1971). A particularly interesting solution is that explicitly deduced by Yokel (1971) for a prismatic beam-column made up of a no tension material with infinite compressive strength loaded by an axial force applied at both ends.

In the present work Yokel's results have been generalised to the case of a no-tension material with bounded deformability and compressive strength. Although quite complex because of the introduction of further constitutive non-linearities, such a generalisation makes this model more suitable to describing the stability of some masonry piles loaded by a normal force acting eccentrically. As in Yokel (1971), we have limited the study to piles with rectangular cross sections subjected to a normal force acting within the cross section, and outside its middle-third; the case of a normal force acting within the middle third of the pile's end sections will be taken up in a subsequent work.

Firstly, we present the main characteristics of the original constitutive equation and we define the distribution of the axial stress component in the section as a function of the internal forces. A further development of this topic is presented in Zani (2001).

Subsequently, the differential equation for the deformed shape of the compressed fibre of the pile is developed. Explicit solution of this equation yields a load–displacement relation from which we can deduce the stability characteristics of the pile, suitably represented by response curves. Then, we determine to what extent an imposed limit to the maximum permissible strain on the material under compression reduces the admissible range of the response curves obtained. Finally, we present an application of this model and show how to calculate a load reduction factor, useful for checking masonry column subjected to eccentric vertical loading.

2. The domain of admissible internal forces in the case of a no-tension material with limited compressive strength and deformability

Firstly, we need to determine the distribution of the axial stress component in any given section of the pile (Fig. 1(a)) as a function of the axial force, N, and the bending moment, M, under the assumptions dictated by the constitutive model for uniaxial stresses shown in Fig. 1(b).

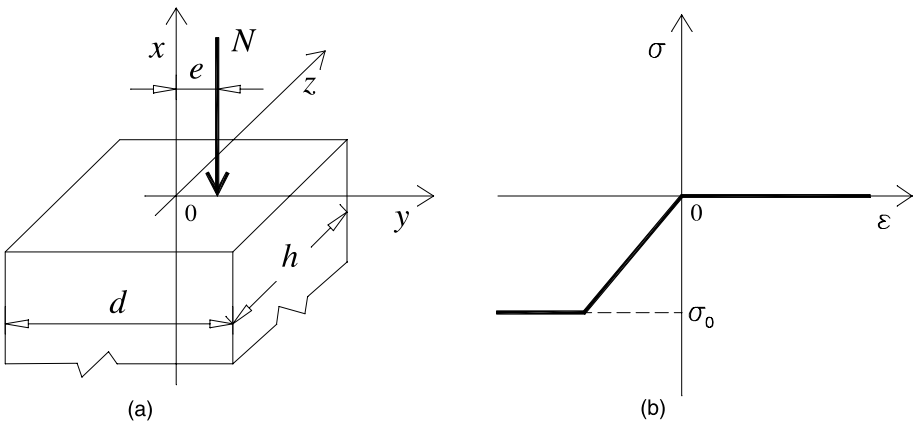

Fig. 1. (a) Pile section loaded by a normal force acting with eccentricity e. (b) Material constitutive model for uniaxial stress.

Let us indicate as d and h the external dimensions of any given cross section of the pile, and set

$$\overline{N} = \frac{N}{hd\sigma_0} \quad \text{and} \quad \overline{M} = \frac{M}{hd^2\sigma_0}, \tag{1}$$

with σ_0 (<0), the limit compressive stress of the material. It is well known that, in order for the axial component σ of the stress to satisfy the inequality $\sigma_0 \leqslant \sigma \leqslant 0$ at each point in the section, $(\overline{N}, \overline{M})$ must belong to the region

$$\Omega = \left\{ (\overline{N}, \overline{M}) \,|\, 0 \leqslant \overline{N} \leqslant 1,\ |\overline{M}| \leqslant \frac{\overline{N}}{2}(\overline{N} - 1) \right\}. \tag{2}$$

Under the Euler–Bernoulli hypothesis, for each $(\overline{N}, \overline{M}) \in \Omega$, the distribution of the axial stress component in the section can be represented as in Fig. 2. It can therefore be thoroughly characterised by parameters a and b, which represent the lengths of the segments where the stress is constant and linear, respectively. By reason of symmetry, we can limit ourselves to specifying parameters a and b for the couples $(\overline{N}, \overline{M})$, belonging to the region $\Omega^+ = \{(\overline{N}, \overline{M}) \in \Omega \,|\, \overline{M} \geqslant 0\}$.

To this end, it is helpful to consider the partition of Ω^+ made up of the open and disjoint subsets shown in Fig. 3. These are bounded by the curves

$$\Gamma = \left\{ (\overline{N}, \overline{M}) \,|\, 0 \leqslant \overline{N} \leqslant 1,\ \overline{M} = \frac{\overline{N}}{2}(\overline{N} - 1) \right\}, \tag{3}$$

$$\alpha = \left\{ (\overline{N}, \overline{M}) \,|\, 0 \leqslant \overline{N} \leqslant \frac{1}{2},\ \overline{M} = -\frac{2}{3}\overline{N}^2 + \frac{1}{2}\overline{N} \right\}, \tag{4}$$

$$\beta = \left\{ (\overline{N}, \overline{M}) \,|\, \frac{1}{2} \leqslant \overline{N} \leqslant 1,\ \overline{M} = -\frac{2}{3}\overline{N}^2 + \frac{5}{6}\overline{N} - \frac{1}{6} \right\}, \tag{5}$$

$$r_1 = \left\{ (\overline{N}, \overline{M}) \,|\, 0 \leqslant \overline{N} \leqslant \frac{1}{2},\ \overline{M} = \frac{1}{6}\overline{N} \right\}, \tag{6}$$

$$r_2 = \left\{ (\overline{N}, \overline{M}) \,|\, \frac{1}{2} \leqslant \overline{N} \leqslant 1,\ \overline{M} = \frac{1}{6}(1 - \overline{N}) \right\}. \tag{7}$$

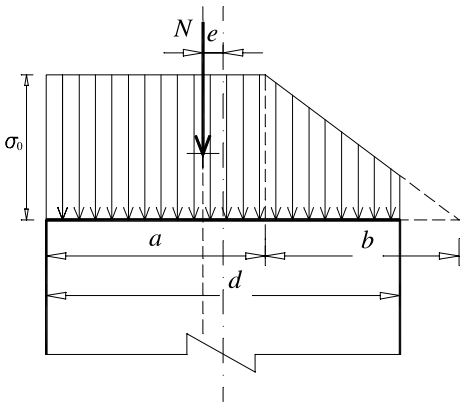

Fig. 2. Stress distribution in the pile section.

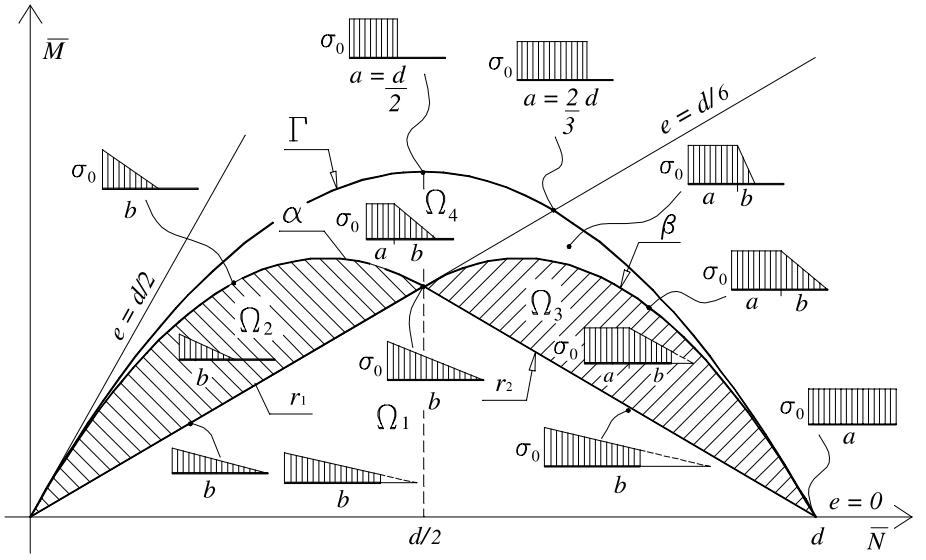

Fig. 3. Stress distribution in the regions of the admissible range.

In fact, it can be verified that

$$(\overline{N},\overline{M}) \in \Omega_1 \Rightarrow a = 0 \quad \text{and} \quad b = \frac{d\overline{N}}{12\overline{M}} + \frac{d}{2}, \tag{8}$$

$$(\overline{N},\overline{M}) \in \Omega_2 \Rightarrow a = 0 \quad \text{and} \quad b = 3d\left(\frac{1}{2} - \frac{\overline{M}}{\overline{N}}\right), \tag{9}$$

$$(\overline{N},\overline{M}) \in \Omega_3 \Rightarrow a = \frac{d\left(-1+\overline{N}+6\overline{M}\right)}{2\left(1-\overline{N}\right)} \quad \text{and} \quad b = \frac{9d(-1+\overline{N}+2\overline{M})^2}{8(1-\overline{N})^3} \quad (\text{for } \overline{N} \neq 1), \tag{10}$$

$$(\overline{N},\overline{M}) \in \Omega_4 \Rightarrow a = d\left(\overline{N} - \sqrt{-3\overline{N}^2 + 3\overline{N} - 6\overline{M}}\right) \quad \text{and} \quad b = 2d\sqrt{-3\overline{N}^2 + 3\overline{N} - 6\overline{M}}. \tag{11}$$

In order to account for the material's limited deformability as well, we assume the constitutive relation described in Fig. 4(a), where ε_u (<0) is the limit compressive strain. For $\varepsilon = \varepsilon_u$, cracks are produced in the more compressed portion of the section.

Let E be Young's modulus for the material under compression; under the Euler–Bernoulli hypothesis, with $\varepsilon_0 = \sigma_0/E$ the strain corresponding to the limit compressive stress on the section, we have (Fig. 4(b))

$$\varepsilon_m = \frac{\sigma_0}{E}\frac{(a+b)}{b}, \tag{12}$$

where ε_m is the minimum strain on the section.

Therefore, by setting

$$k = \frac{\varepsilon_u}{\varepsilon_0}, \tag{13}$$

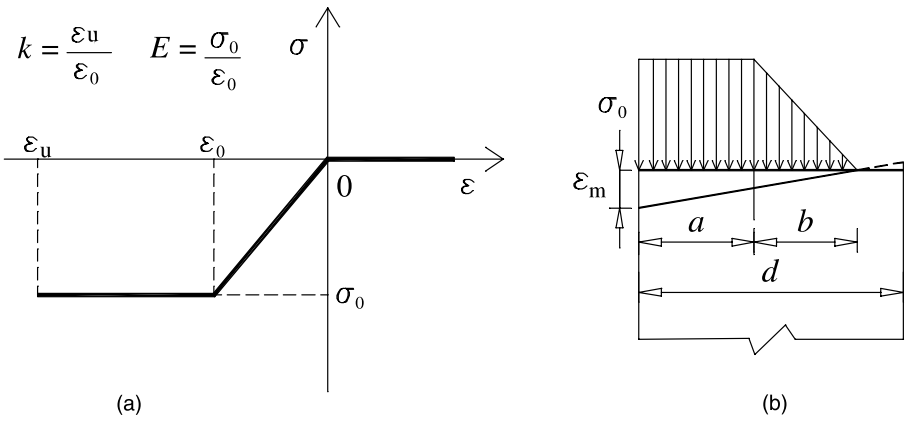

Fig. 4. (a) Constitutive equation of the material for monoaxial stress states. (b) Strain pattern in the cross section.

for $(\overline{N},\overline{M}) \in \Omega_4$, in light of (11) and (12) and with $\varepsilon_m = \varepsilon_u$, from (13), we obtain the relation

$$\overline{M} = \frac{3\overline{N}(2k-1)^2 - 4\overline{N}^2(3k^2-3k+1)}{6(2k-1)^2}. \tag{14}$$

While, for $(\overline{N},\overline{M}) \in \Omega_3$, in light of (10) and (12), once again from (13) we obtain

$$\overline{M} = \begin{cases} \frac{(1-\overline{N})\left(2\sqrt{(1-\overline{N})((2k-1)-\overline{N})}+(1-3k)+2\overline{N}\right)}{6(1-k)} & \text{for} \quad k > 1, \\ \frac{1}{6}(1-\overline{N}) & \text{for} \quad k = 1. \end{cases} \tag{15}$$

The curves delineated by (14) and (15) on the plane $(\overline{N},\overline{M})$ have been plotted in Fig. 5 and represent the boundary of the admissible range for each value of k.

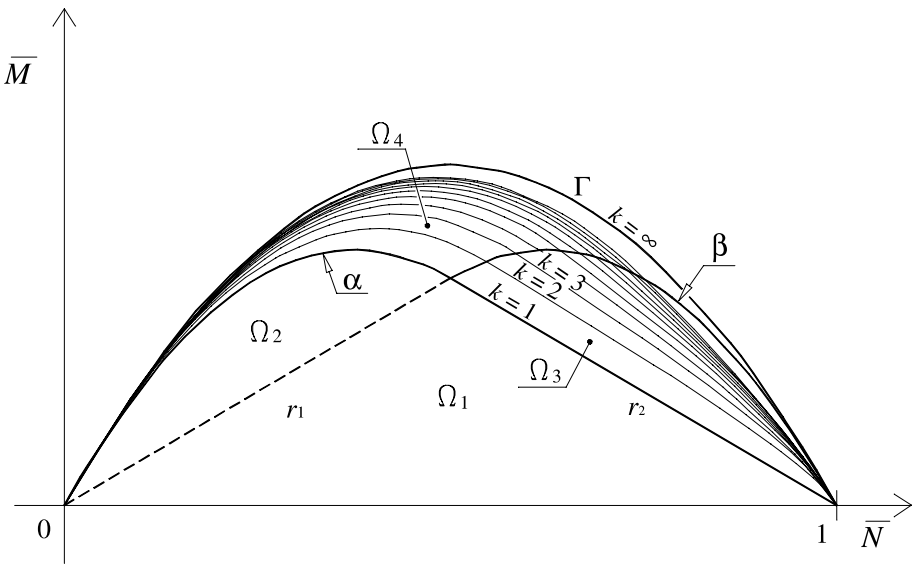

Fig. 5. Boundary of the admissible range for each k.

Of course, for $k = 1$, Eqs. (14) and (15) coincide with (4) and (5), respectively, the equations of curves α and β, while for k tending towards infinity, Eq. (14) tends to coincide with Eq. (3), the equation of the boundary Γ of domain Ω^+.

3. The pile loaded by an eccentric axial load

Let us now consider a pile of height $2L$, made up of a no-tension material with limited compressive strength and deformability, loaded by an axial load N applied at both end sections, parallel to, and at distance e from the undeformed axis of the pile (Fig. 6). Both extremities are restrained with two hinges: as shown in Fig. 6, the hinge where the load N is applied has the degree of freedom of vertical displacement.

Assuming, as always, that the cross sections remain plane and orthogonal to the deformed axis of the pile, the strain has a linear pattern on the section. Moreover, since we suppose the load N to be acting outside the middle third of the top section, we have $d/6 \leqslant e < d/2$, and cracking occurs in all sections.

Let u be the distance of the load's line of action from the compressed edge of the section; because of bending, u varies along the pile's height and attains its maximum value u_L at the summit, and its minimum u_0 in the middle section, where the stress at the compressed border of the section moreover reaches its maximum value.

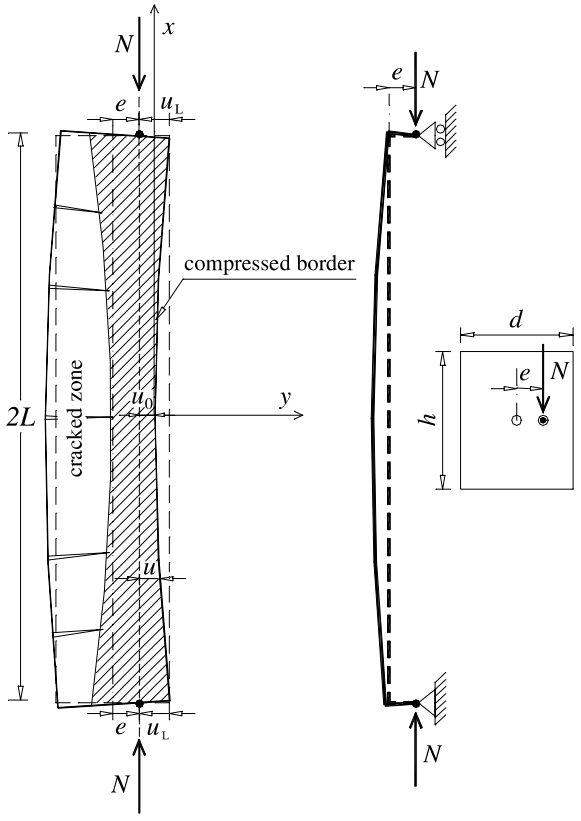

Fig. 6. Scheme used to study the pile.

Following the procedure set forth by Yokel (1971), in order to obtain the deformed shape of the pile, it is more convenient to refer to the compressed border of the pile, rather than its barycentric axis. To this end, let us adopt the coordinate system (o,x,y) shown in Fig. 6, in which the origin is at the middle and the x-axis is tangential to the most compressed fibre of the pile and parallel to the load's line of action. Moreover, we set

$$y(x) = u(x) - u_0, \tag{16}$$

so that $y(L) = u_L - u_0$, where the value of $u_L = d/2 - e_L$ is known.

During the loading process, as the load intensity increases, all sections become cracked.

If failure does not come about by instability due to buckling of the beam, the compressive stress will reach the limit value σ_0, first at the middle section and subsequently in a growing segment of the pile extending upward to the summit.

Now, let N_0 and N_L be the values of N in correspondence to which the compressive stress reaches the value of σ_0 at the middle section and at the summit of the pile, respectively. By virtue of the hypothesis that the cross sections remain plane and orthogonal to the undeformed axis of the pile, together with the assumed elastic response of the material all the way up to the maximum compressive stress σ_0, we can easily verify that

$$\overline{N}_0 = \frac{3}{2}\frac{u_0}{d}, \quad \overline{N}_L = \frac{3}{2}\frac{u_L}{d}, \tag{17}$$

so that $\overline{N}_L > \overline{N}_0$ always holds. Finally, let N_k be the maximum value of N compatible with the ductility expressed by the ratio k, that is, the value in correspondence to which the ultimate strain ε_u is equal to $k\varepsilon_0$.

By substituting $M = N(d/2 - u_0)$ into (14), with the positions (1), we obtain

$$\overline{N}_k = \frac{6(2k-1)^2}{1+3(2k-1)^2}\frac{u_0}{d}. \tag{18}$$

As k tends to infinity, N_k tends towards the value

$$\overline{N}_u = 2\frac{u_0}{d}. \tag{19}$$

By equilibrium considerations, it is an easy matter to deduce that N_u is the value of N in correspondence to which the stress distribution at the middle section takes on the constant value σ_0. N_u is thus the maximum value that N can attain, and this comes about when the internal forces $(\overline{N},\overline{M})$ at the middle section of the column represent a point on the boundary Γ of the admissible domain.

Contrary to N_L, the values of N_u, N_k and N_0 cannot be determined a priori once we know the load eccentricity at the summit, the geometrical dimensions of the pile and the mechanical characteristics of the material. However, their values can be deduced through a relation between N and u_0 which we now intend to determine.

For $N < N_0$, the compressive stress does not attain the maximum value σ_0 in any section of the pile; under such circumstances, the stress distribution in the section is typical of region Ω_2, and Yokel's relation (see, for example, Yokel, 1971) between N and u_0 holds:

$$\frac{N}{N_{\text{eq}}} = 0.40528\alpha\left[\sqrt{1-\alpha} + \alpha\ln\left(\sqrt{\frac{1-\alpha}{\alpha}} + \sqrt{\frac{1}{\alpha}}\right)\right]^2, \tag{20}$$

where $N_{\text{eq}} = -9\pi^2 E h u_L^3/16L^2$ is the critical load of the compressed zone of the top section and $\alpha = u_0/u_L$ is a measure of the relative lateral displacement between the middle and the end section. The behaviour of N/N_{eq} as a function of α is shown in Fig. 7.

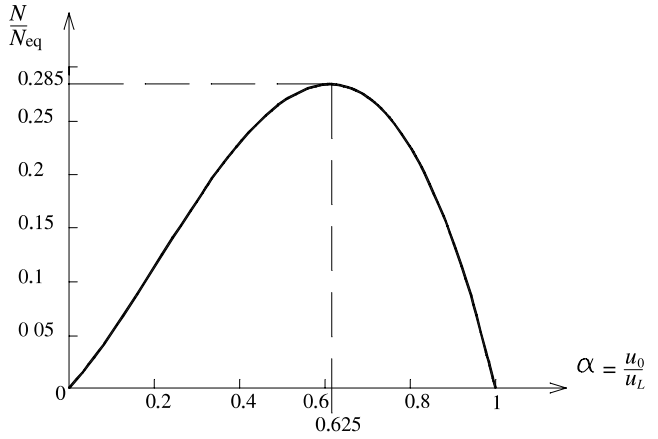

Fig. 7. Curve obtained by Yokel (1971) (Eq. (20)).

It can be seen that every value of N/N_{eq} has two corresponding values of α; in particular, for $N/N_{eq} = 0$, $\alpha = 1$ represents the undeformed case ($u_0 = u_L$), and $\alpha = 0$ the case in which u_0 vanishes, which happens when the load's line of action is tangent to the compressed border of the middle section. In the right branch of the curve, that is, for $0.625 < \alpha \leqslant 1$, which corresponds to a condition of stable equilibrium, we may observe that as N increases, the deformation of the pile increases as well; thus u_0 decreases, and with it, α as well. For $\alpha = 0.625$, the maximum load, $N_{cr} = 0.285N_{eq}$ bearable by the pile is reached. Values of N/N_{eq} in the interval $0 \leqslant \alpha \leqslant 0.625$ are lacking of interest to applications because they correspond to large deformation values that occur for loads smaller than the critical one, in an unstable equilibrium state.

Let us now suppose that $N \geqslant N_0$ and denote s as the maximum ordinate at which the stress value at the section's compressed border equals σ_0.

Note that for $N_0 < N < N_L$, $s < L$. Thus, the half-pile is divided into the two segments, $0 < x \leqslant s$ and $s < x < L$, each of which is characterised by a local load distribution typical of regions Ω_4 and Ω_2, respectively (see Fig. 8). For $N > N_L$ we instead have $s > L$, and the stress distribution in all sections of the pile is that typical of region Ω_4.

Denoting $u(s)$ as the distance of the load's line of action from the compressed edge of the section at height $x = s$, from considerations of equilibrium, it follows that

$$u(s) = \frac{2}{3}\overline{N}d. \tag{21}$$

During the loading process, the internal forces relative to any given cross section describe a curve on the plane $(\overline{N}, \overline{M})$. Fig. 9 shows curves c_0 and c_L for the middle and top sections, respectively.

It can be seen that as $\overline{N}$ increases, the concavity of curve c_0 turns upward up to the value $\overline{N}_{cr}$, which represents the maximum load the pile can bear under stable equilibrium conditions. The subsequent branch then shows decreasing values of $\overline{N}$.

The loading process finishes when curve c_0 intersects the ductility curve relative to the characteristic value of k for the material; thus, we assume that the crisis of the pile takes place, as soon as the compressive strain at the middle section attains its limit value ε_u. In particular, for $k = 1$, curve c_0 ends on α, while for $k = \infty$, it ends on the boundary Γ of domain Ω^+.

Thus, in this model failure is assumed to take place either because the limit compressive strain is reached or by instability, depending on whether c_0 intersects the material's characteristic k-value curve for $\overline{N} < \overline{N}_{cr}$.

The next step is to determine the relation between load N and distance u_0 for $\overline{N} \geqslant \overline{N}_0$, as well.

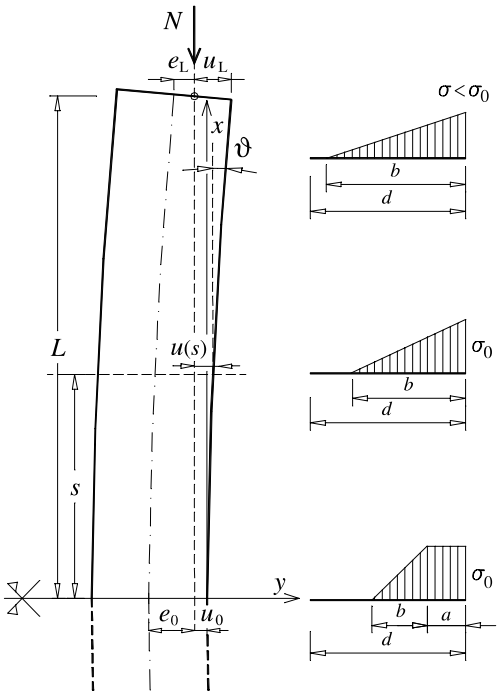

Fig. 8. For $N \geqslant N_0$, the pile is divided into two segments, each corresponding to a stress distribution.

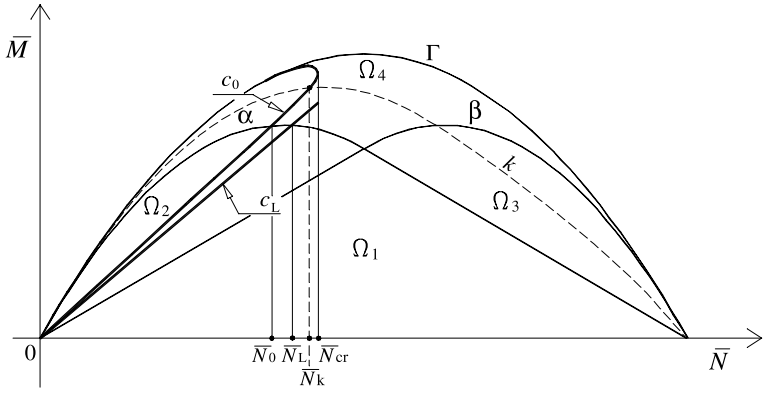

Fig. 9. Curves c_0 and c_L relative to the middle and top sections.

To this end, let us set

$$u = \begin{cases} u_1 & \text{for } s < x \leqslant L, \\ u_2 & \text{for } 0 \leqslant x \leqslant s, \end{cases} \tag{22}$$

and consider an infinitesimally small element of the pile set at height x (Fig. 10). The length of the compressed zone is equal to $a + b$, with a and b determined by relation (11).

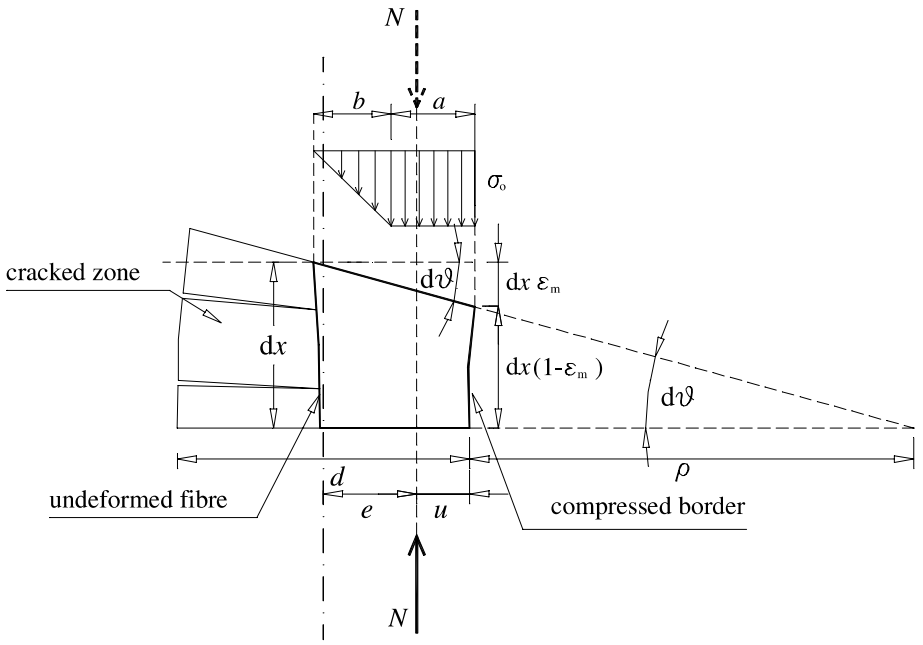

Fig. 10. Infinitesimal beam element in $0 \leqslant x \leqslant s$.

From simple geometrical considerations, we can deduce that

$$\frac{\mathrm{d}\vartheta}{\mathrm{d}x} = \frac{\varepsilon_m}{a+b}, \tag{23}$$

where, as usual, ε_m is the strain of the most compressed edge, and $\mathrm{d}\vartheta$ is the relative rotation between the two end sections of the element.

By virtue of the hypothesis that all sections remain plane, we have

$$\varepsilon_m = \varepsilon_b \frac{(a+b)}{b}, \tag{24}$$

where ε_b is the strain of the fibre at distance b from the neutral axis, and

$$\varepsilon_b = \frac{\sigma_{\min}}{E} \quad \text{for } s < x \leqslant L \text{ (region } \Omega_2) \quad \text{and} \quad \varepsilon_b = \frac{\sigma_0}{E} \quad \text{for } 0 \leqslant x \leqslant s \text{ (region } \Omega_4), \tag{25}$$

with $\sigma_{\min}$ the minimum compressive stress in the section.

Expressing $\mathrm{d}\vartheta/\mathrm{d}x$ as a function of ρ, the curvature radius of the compressed pile fibre, we can obtain its change in slope

$$\frac{\mathrm{d}\vartheta}{\mathrm{d}x} = \frac{(1-\varepsilon_m)}{a+b+\rho}. \tag{26}$$

By equating (26) to (23) and neglecting ε_m with respect to the unit, in light of (24) and (25), with $\sigma_{\min} = 2\overline{N}d\sigma_0/b$, we have

$$\rho = \frac{1}{2}\frac{Eb^2}{\overline{N}d\sigma_0} \text{ for } s < x \leqslant L \text{ (region } \Omega_2) \quad \text{and} \quad \rho = \frac{Eb}{\sigma_0} \text{ for } 0 \leqslant x \leqslant s \text{ (region } \Omega_4). \tag{27}$$

Moreover, as usual, let

$$\frac{1}{\rho} = -\frac{\mathrm{d}^2 y}{\mathrm{d}x^2}, \tag{28}$$

where $y(x) = u(x) - u_0$ is the transverse displacement of the compressed fibre. In light of (11) and (9), from (27) we can deduce

$$\begin{cases} \dfrac{\mathrm{d}^2 u_1}{\mathrm{d}x^2} = -\dfrac{2\overline{N} d\sigma_0}{9E}\dfrac{1}{u_1^2} & \text{for } s < x \leqslant L, \\ \dfrac{\mathrm{d}^2 u_2}{\mathrm{d}x^2} = -\dfrac{\sigma_0}{2Ed}\dfrac{1}{\sqrt{3\overline{N}\left(2\frac{u_2}{d} - \overline{N}\right)}} & \text{for } 0 \leqslant x \leqslant s, \end{cases} \tag{29}$$

with the conditions

$$\frac{\mathrm{d}u_2}{\mathrm{d}x}(0) = 0, \quad \frac{\mathrm{d}u_2}{\mathrm{d}x}(s) = \vartheta(s), \quad u_2(s) = \frac{2}{3} d\overline{N}, \tag{30}$$

$$u_1(s) = \frac{2}{3} d\overline{N}, \quad \frac{\mathrm{d}u_1}{\mathrm{d}x}(s) = \vartheta(s), \quad u_1(L) = u_L, \tag{31}$$

(see Fig. 8), where $\vartheta(s)$ represents the rotation of the fibre at the compressed edge for $x = s$.

Conditions $(30)_1$ and $(31)_3$ respectively impose that the tangent to the compressed border of the pile at the middle section be vertical, and that the distance of the load's line of action from the compressed edge at the top section be u_L. Both conditions assign the variables known values in a known position. Relations $(30)_3$ and $(31)_1$ dictate continuity of the fibre at the compressed border at connection point $x = s$, and assign known values at sections whose positions are unknown. Finally, in $(30)_2$ and $(31)_2$, which express the continuity of fibre rotation at the compressed border for $x = s$, both the assigned values and the sections' positions are unknown.

As our goal is to determine the relationship between the load parameter $\overline{N}$ and u_0, we do not integrate Eqs. $(29)_1$ and $(29)_2$ with conditions (30) and (31). Instead, we first integrate Eq. $(29)_2$ with condition $(30)_1$, supposing the distance u_0 of the load's line of action from the compressed border of the middle section to be known. In this way we obtain, $\mathrm{d}u_2/\mathrm{d}x$ and x as a function of u_2 for every $\overline{N}$. We thereby deduce the values of $\vartheta(s)$ and s from conditions $(30)_2$ and $(30)_3$.

Subsequently, Eq. $(29)_1$ will be integrated with the two conditions, $(31)_1$ and $(31)_2$, and x determined as a function of u_1. Finally, by imposing condition $(31)_3$, i.e., the top-section condition, we can arrive at the desired relation between $\overline{N}$ and u_0.

Thus, multiplying both members of $(29)_2$ by $2\,\mathrm{d}u_2/\mathrm{d}x$ and integrating between 0 and x with condition $(30)_1$ and the additional condition $u_2(0) = u_0$, we obtain

$$\left(\frac{\mathrm{d}u_2}{\mathrm{d}x}\right)^2 = \frac{-\sigma_0}{Ed\sqrt{3\overline{N}}}\left(\sqrt{2\frac{u_2}{d} - \overline{N}} - \sqrt{2\frac{u_0}{d} - \overline{N}}\right), \tag{32}$$

from which

$$\frac{\mathrm{d}x}{\mathrm{d}u_2} = \frac{1}{\sqrt{\frac{-\sigma_0}{Ed\sqrt{3\overline{N}}}\left(\sqrt{2\frac{u_2}{d} - \overline{N}} - \sqrt{2\frac{u_0}{d} - \overline{N}}\right)}}. \tag{33}$$

Integrating this equation by separation of variables, we can easily obtain

$$x = \frac{2}{3} d\sqrt{-\frac{E\sqrt{3\overline{N}}}{\sigma_0}\left(\sqrt{2\frac{u_2}{d} - \overline{N}} - \sqrt{2\frac{u_0}{d} - \overline{N}}\right)}\left(5\sqrt{2\frac{u_0}{d} - \overline{N}} - 2\sqrt{2\frac{u_2}{d} - \overline{N}}\right). \tag{34}$$

Now imposing condition $(30)_3$, we obtain the value of x in correspondence to which compression σ_0 is reached only at one point of the section's compressed edge. We thus have

$$s = \frac{2}{3}d\sqrt{-\frac{E\sqrt{3\overline{N}}}{\sigma_0}\left(\sqrt{\frac{\overline{N}}{3}}-\sqrt{2\frac{u_0}{d}-\overline{N}}\right)}\left(-2\sqrt{\frac{\overline{N}}{3}}+5\sqrt{2\frac{u_0}{d}-\overline{N}}\right). \tag{35}$$

Now, from (32), in light of (35), and by imposing condition $(30)_2$, we can deduce the rotation of the section at height s,

$$\vartheta(s) = \sqrt{-\frac{\sigma_0}{E\sqrt{3\overline{N}}}\left(\sqrt{\frac{\overline{N}}{3}}-\sqrt{2\frac{u_0}{d}-\overline{N}}\right)}. \tag{36}$$

In order to integrate $(29)_1$, we multiply both members by $2\,\mathrm{d}u_1/\mathrm{d}x$ and impose condition $(31)_2$, thereby obtaining

$$\frac{\mathrm{d}u_1}{\mathrm{d}x} = \sqrt{-\frac{4}{9}\frac{\overline{N}\sigma_0}{E}\left(\frac{3}{2\overline{N}}-\frac{d}{u_1}\right)+\vartheta^2}. \tag{37}$$

Using the method of separation of variables, we integrate both members of (37) between s and x with the change in variable

$$t = \sqrt{\frac{u_1}{\gamma u_1 - d\beta}}, \tag{38}$$

where $\gamma = 3(-2\sigma_0 + 3E\vartheta^2)$ and $\beta = -4\overline{N}\sigma_0$.

Integrating the second member of (37) by parts, and setting

$$\frac{1}{1-\gamma t^2} = \frac{1}{2(1+\sqrt{\gamma}t)} + \frac{1}{2(1-\sqrt{\gamma}t)}, \tag{39}$$

in light of $(31)_1$, we obtain

$$x = 3d\sqrt{E}\frac{\beta}{\gamma}\left[t\left(\frac{1}{\gamma t^2-1}\right)+\frac{1}{2\sqrt{\gamma}}\ln\frac{1+\sqrt{\gamma}t}{1-\sqrt{\gamma}t}\right]_{t(s)}^{t(x)} + s, \tag{40}$$

which, by virtue of (38) and (39) gives

$$x = -d\sqrt{E}\frac{4\overline{N}\sigma_0}{(-2\sigma_0+3E\vartheta^2)}\left[\frac{\sqrt{(-6\sigma_0+9E\vartheta^2)u_1^2+4\overline{N}\sigma_0 du_1}}{-4d\overline{N}\sigma_0}\right.$$
$$\left.+\frac{1}{2\sqrt{3(-2\sigma_0+3E\vartheta^2)}}\ln\frac{\sqrt{(-6\sigma_0+9E\vartheta^2)u_1+4d\overline{N}\sigma_0}+\sqrt{(-6\sigma_0+9E\vartheta^2)u_1}}{\left|\sqrt{(-6\sigma_0+9E\vartheta^2)u_1+4d\overline{N}\sigma_0}-\sqrt{(-6\sigma_0+9E\vartheta^2)u_1}\right|}\right]_{u_1(s)}^{u_1(x)} + s. \tag{41}$$

By substituting the integration limits, we have

$$x = -\sqrt{E}\frac{4d\overline{N}\sigma_0}{(-2\sigma_0+3E\vartheta^2)}\left\{\left[\frac{\sqrt{(-6\sigma_0+9E\vartheta^2)u_1^2+4d\overline{N}\sigma_0 u_1}}{-4d\overline{N}\sigma_0}\right.\right.$$
$$\left.+\frac{1}{2\sqrt{3(-2\sigma_0+3E\vartheta^2)}}\ln\frac{\sqrt{(-6\sigma_0+9E\vartheta^2)u_1+4d\overline{N}\sigma_0}+\sqrt{(-6\sigma_0+9E\vartheta^2)u_1}}{\left|\sqrt{(-6\sigma_0+9E\vartheta^2)u_1+4d\overline{N}\sigma_0}-\sqrt{(-6\sigma_0+9E\vartheta^2)u_1}\right|}\right]$$
$$\left.-\left[-\frac{\vartheta\sqrt{E}}{2\sigma_0}+\frac{1}{2\sqrt{3(-2\sigma_0+3E\vartheta^2)}}\ln\frac{\sqrt{6\overline{N}E\vartheta^2}+\sqrt{(-2\sigma_0+3E\vartheta^2)2\overline{N}}}{\left|\sqrt{6\overline{N}E\vartheta^2}-\sqrt{(-2\sigma_0+3E\vartheta^2)2\overline{N}}\right|}\right]\right\}+s. \tag{42}$$

By then imposing condition $(31)_3$, relation (42) furnishes the desired relationship between $\overline{N}$ and u_0,

$$-\sqrt{E}\frac{4d\overline{N}\sigma_0}{(-2\sigma_0+3E\vartheta^2)}\left\{\left[\frac{\sqrt{(-6\sigma_0+9E\vartheta^2)u_L^2+4d\overline{N}\sigma_0 u_L}}{-4d\overline{N}\sigma_0}\right.\right.$$
$$\left.+\frac{1}{2\sqrt{3(-2\sigma_0+3E\vartheta^2)}}\ln\frac{\sqrt{(-6\sigma_0+9E\vartheta^2)u_L+4d\overline{N}\sigma_0}+\sqrt{(-6\sigma_0+9E\vartheta^2)u_L}}{\left|\sqrt{(-6\sigma_0+9E\vartheta^2)u_L+4d\overline{N}\sigma_0}-\sqrt{(-6\sigma_0+9E\vartheta^2)u_L}\right|}\right]$$
$$\left.-\left[-\frac{\vartheta\sqrt{E}}{2\sigma_0}+\frac{1}{2\sqrt{3(-2\sigma_0+3E\vartheta^2)}}\ln\frac{\sqrt{6\overline{N}E\vartheta^2}+\sqrt{(-2\sigma_0+3E\vartheta^2)2\overline{N}}}{\left|\sqrt{6\overline{N}E\vartheta^2}-\sqrt{(-2\sigma_0+3E\vartheta^2)2\overline{N}}\right|}\right]\right\}+s-L=0. \tag{43}$$

The last relation can be conveniently written in dimensionless form. In fact, by indicating as $N_E=\pi^2EJ/4L^2$ the critical Eulerian load of a pile made of linear elastic material (Fig. 8), we have

$$\overline{N}=\frac{\pi^2}{12}\frac{n^2}{\lambda^2}, \tag{44}$$

with

$$n^2=\frac{N}{N_E},\quad \lambda=\frac{2L}{d}\sqrt{\frac{\sigma_0}{E}}, \tag{45}$$

where parameters n and λ are dimensionless: the first expresses the ratio between applied load and the corresponding Eulerian critical load, while the second, which summarises all the beam's geometric and mechanical properties, can be interpreted as a measure of its slenderness.

In light of (44) and (45), and by putting

$$\alpha_0=\frac{u_0}{d},\quad \alpha_L=\frac{u_L}{d},\quad m=-\frac{E}{\sigma_0}, \tag{46}$$

relations (35), (36) and (43) become

$$s=\frac{2}{3}d\pi^2\frac{n^2}{\lambda^2}\sqrt{\frac{m}{2}\left(\frac{1}{6}-\sqrt{2\alpha_0\frac{\lambda^2}{\pi^2n^2}-\frac{1}{12}}\right)}\left(-\frac{1}{3}+5\sqrt{2\alpha_0\frac{\lambda^2}{\pi^2n^2}-\frac{1}{12}}\right), \tag{47}$$

$$\vartheta(s)=\sqrt{\frac{1}{m}\left(\frac{1}{3}-2\sqrt{2\alpha_0\frac{\lambda^2}{\pi^2n^2}-\frac{1}{12}}\right)}. \tag{48}$$

$$\sqrt{m}\frac{\frac{\pi^2}{3}\frac{n^2}{\lambda^2}}{3\left(1-2\sqrt{2\alpha_0\frac{\lambda^2}{\pi^2n^2}-\frac{1}{12}}\right)}\left\{\frac{\sqrt{9\left(1-2\sqrt{2\alpha_0\frac{\lambda^2}{\pi^2n^2}-\frac{1}{12}}\right)\alpha_L^2-\frac{\pi^2}{3}\frac{n^2}{\lambda^2}\alpha_L}}{\frac{\pi^2}{3}\frac{n^2}{\lambda^2}}\right.$$
$$+\frac{1}{6\sqrt{\left(1-2\sqrt{2\alpha_0\frac{\lambda^2}{\pi^2n^2}-\frac{1}{12}}\right)}}\left[\ln\frac{\sqrt{9\left(1-2\sqrt{2\alpha_0\frac{\lambda^2}{\pi^2n^2}-\frac{1}{12}}\right)\alpha_L-\frac{\pi^2}{3}\frac{n^2}{\lambda^2}}+\sqrt{9\left(1-2\sqrt{2\alpha_0\frac{\lambda^2}{\pi^2n^2}-\frac{1}{12}}\right)\alpha_L}}{\left|\sqrt{9\left(1-2\sqrt{2\alpha_0\frac{\lambda^2}{\pi^2n^2}-\frac{1}{12}}\right)\alpha_L-\frac{\pi^2}{3}\frac{n^2}{\lambda^2}}-\sqrt{9\left(1-2\sqrt{2\alpha_0\frac{\lambda^2}{\pi^2n^2}-\frac{1}{12}}\right)\alpha_L}\right|}\right.$$
$$\left.\left.-\ln\frac{\sqrt{\frac{1}{3}-2\sqrt{2\alpha_0\frac{\lambda^2}{\pi^2n^2}-\frac{1}{12}}}+\sqrt{1-2\sqrt{2\alpha_0\frac{\lambda^2}{\pi^2n^2}-\frac{1}{12}}}}{\left|\sqrt{\frac{1}{3}-2\sqrt{2\alpha_0\frac{\lambda^2}{\pi^2n^2}-\frac{1}{12}}}-\sqrt{1-2\sqrt{2\alpha_0\frac{\lambda^2}{\pi^2n^2}-\frac{1}{12}}}\right|}\right]-\sqrt{\left(\frac{1}{12}-\frac{1}{2}\sqrt{2\alpha_0\frac{\lambda^2}{\pi^2n^2}-\frac{1}{12}}\right)}\right\}+\frac{s}{d}-\frac{L}{d}=0. \tag{49}$$

And finally, by setting

$$\beta_0=1-2\sqrt{2\alpha_0\frac{\lambda^2}{\pi^2n^2}-\frac{1}{12}},\quad \delta=\frac{L}{d}-\frac{s}{d},\quad \gamma=\frac{\pi^2n^2}{3\lambda^2}, \tag{50}$$

from (47)–(49), we have

$$s=d\frac{\gamma}{2}\sqrt{\frac{m}{3}(3\beta_0-2)}\left(\frac{13}{3}-5\beta_0\right), \tag{51}$$

$$\vartheta(s)=\sqrt{\frac{(3\beta_0-2)}{3m}}, \tag{52}$$

$$\frac{\gamma\sqrt{m}}{6\beta_0}\left\{-\frac{2\sqrt{9\beta_0\alpha_L^2-\gamma\alpha_L}}{\gamma}+\frac{1}{3\sqrt{\beta_0}}\ln\frac{\left(\sqrt{9\beta_0\alpha_L-\gamma}+\sqrt{9\beta_0\alpha_L}\right)\left(\sqrt{3\beta_0-2}-\sqrt{3\beta_0}\right)}{\left(\sqrt{9\beta_0\alpha_L-\gamma}-\sqrt{9\beta_0\alpha_L}\right)\left(\sqrt{3\beta_0-2}+\sqrt{3\beta_0}\right)}-\sqrt{\left(\beta_0-\frac{2}{3}\right)}\right\}-\delta=0. \tag{53}$$

Of course, in view of (17), (45) and (46), from (53) we deduce that $\delta=0$ for $N=N_L$ and therefore $s=L$.

For $N<N_0$ relation (20), obtained by Yokel (1971) for the case of a normal force acting outside the middle third of the section, with positions (44)–(46), can be written in dimensionless form, for which we obtain

$$n(\alpha_0)=\frac{6\sqrt{3\alpha_0}}{\pi}\alpha_L\left[\sqrt{\frac{\alpha_L-\alpha_0}{\alpha_L}}+\frac{\alpha_0}{\alpha_L}\ln\left(\sqrt{\frac{\alpha_L-\alpha_0}{\alpha_0}}+\sqrt{\frac{\alpha_L}{\alpha_0}}\right)\right]. \tag{54}$$

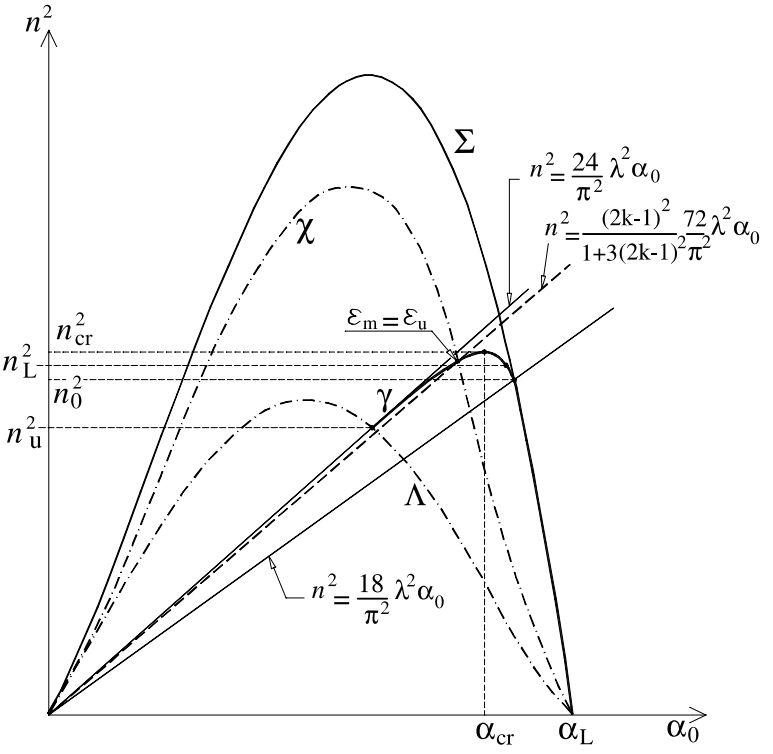

Fig. 11. Analysis of a response curve for $\lambda = 0.325$ and $e_L = d/3.5$.

The response curves, respectively expressed as (53) and (54), when $N \geqslant N_0$ and $N < N_0$, are presented in Fig. 11 for $\alpha_L = \frac{1}{3.5}$ and $k = \infty$.

In particular, observe that, for $\overline{N} = 0$, we have $\alpha_0 = \alpha_L$, and the pile remains undeformed. As $\overline{N}$ increases, we first move along curve Σ, delineated by (54) for a material with infinite compressive strength, until the value $\overline{N} = \overline{N}_0$ is reached. This occurs at $n^2 = n_0^2$ where

$$n_0^2 = \frac{18}{\pi^2}\lambda^2\alpha_0, \tag{55}$$

as can be deduced from (17), with the help of (44)–(46). Then, for any given value of λ, curve Σ loses its meaning when it intersects the line of equation $n^2 = (18/\pi^2)\lambda^2\alpha_0$.

For $\overline{N} \geqslant \overline{N}_0$ (that is, for $n^2 \geqslant n_0^2$), the relation between n^2 and α_0 is represented for each value of λ by a curve, γ, implicitly defined by Eq. (53).

The maximum value n_{cr}^2 of γ is reached when $\alpha_0 = \alpha_{0cr}$, and this is the load value at which the beam collapses due to equilibrium instability before the section can undergo crushing.

The couples (α_{0cr}, n_u^2), relative to different values of λ, may determine a point of either Σ or λ. In the first case, instability of the pile equilibrium takes place when the stress distribution in the section is typical of region Ω_2, however without the stress' reaching the value σ_0 ($n_{cr} \leqslant n_0$) in any section whatsoever. In the second case, instability of the pile equilibrium takes place when compression σ_0 is attained in the pile sections next to the middle and the stress distribution is typical of region Ω_4.

The part of the curve with $\alpha_0 < \alpha_{0cr}$ are of no concern to applications because it corresponds to large deformation values occurring for loads below the critical load, in a state of unstable equilibrium.

For small enough values of λ, curve γ ends when the stress distribution at the middle section of the column takes on the constant value σ_0. This corresponds to the extreme value $\overline{N}_u$, where γ intersects the line whose equation is

$$n^2 = \frac{24}{\pi^2}\lambda^2\alpha_0, \tag{56}$$

as can be deduced from (19), with the help of (44)–(46).

Under such circumstances, the locus of points whose coordinates (α_{0u}, n_u^2) are obtained from the intersection of γ with the line of Eq. (56) is the curve Λ in Fig. 11. The explicit equation of Λ can be obtained by substituting the expression for λ, deduced by Eq. (56), into relation (53). For large enough values of λ, the end points of curves γ belong to Σ.

Moreover, it can be observed that, for a fixed value of α_L, a value $\overline{\lambda}$ exists, such that the critical load for $\lambda \geqslant \overline{\lambda}$ is reached while still along curve Σ. In fact, what occurs is that beyond a certain value of slenderness, collapse of the beam comes about due to instability of the equilibrium, without however the stress ever reaching the value σ_0 in any section whatever.

Finally, with increasing slenderness λ, the response curves γ tend to move along ever more extensive segments of curve Σ, until they are finally superimposed upon it. In other words, from a certain value of λ onwards, the beam behaves as if it were made of a material with infinite compressive strength.

The considerations advanced up to now are valid in the event that the ductility parameter k has an infinite value, as was assumed when drawing Fig. 12, where families of response curves have been represented for $e_L = d/3.5$ and different values of λ.

Instead, when k has a finite value, the validity of curve γ ends at its intersection with the limit curve χ, the locus of points corresponding, for any value of λ, to collapse of the pile by attainment of the ultimate strain.

For any given value of e_L the implicit form of the expression for curve χ, corresponding to any given value of k, is obtained (in a manner analogous to Λ) by calculating the coordinates of the intersection point between curve γ and the line of equation

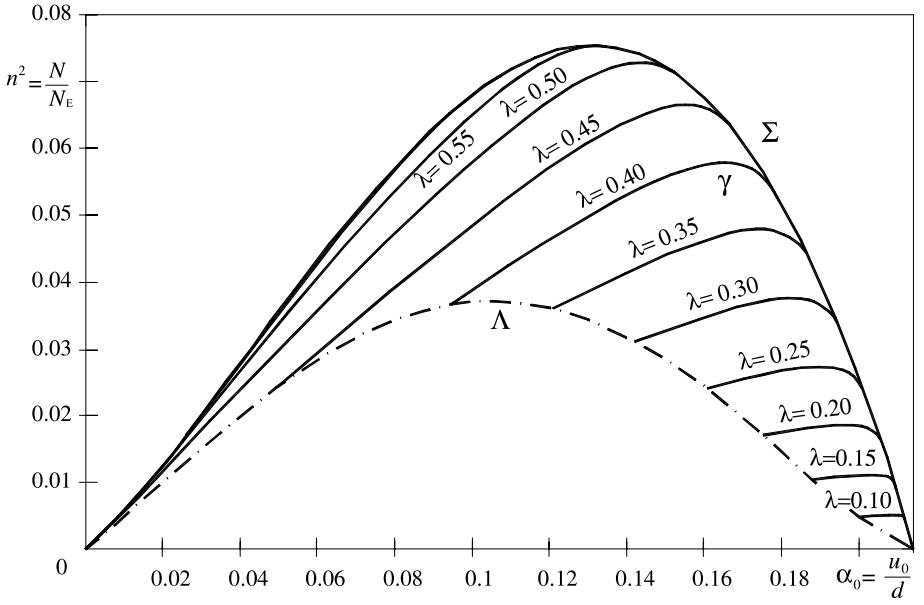

Fig. 12. Response curve family (n^2 versus α_0) for different values of λ and for $e_L = d/3.5$.

$$n^2 = \frac{\lambda^2}{\pi^2} \frac{72(2k-1)^2}{1+3(2k-1)^2} \alpha_0, \tag{57}$$

obtained from (18) with the help (44)–(46).

The family of curves shown in Fig. 13 describes the behaviour of the pile for $k = 1.5$ for two different values of eccentricity at the summit: $e_L = d/3.5$ and $e_L = d/6$.

It can be noticed that, regardless of the eccentricity value e_L, the dashed half-lines of Eq. (57) pass through the extreme points of the γ curves corresponding to the same value of λ.

From the curves in Fig. 13, we can plot the stability curves illustrated in Fig. 14, which show the behaviour of the ratio between failure load N_c and load $N^* = dh\sigma_0$ as a function of parameter λ. The collapse load is represented by the value of either the limit load for instability or the breaking load due to reaching the limit strain, whichever is lower.

In view of (54), with positions (44)–(46), we have

$$\frac{N_c}{N^*} = \frac{\pi^2}{12} \frac{n_c^2}{\lambda^2}, \tag{58}$$

where n_c^2 is the ratio between the collapse load and the Eulerian load of the pile.

For each value of e_L, we present two curves, relative to the values $k = 1$ and $k = \infty$. It can be seen that, for slenderness values tending towards zero, load N_c tends towards the collapse load because the limit strain value is reached. In particular, for $k = 1$, failure occurs when the maximum stress σ_0 is reached at one end

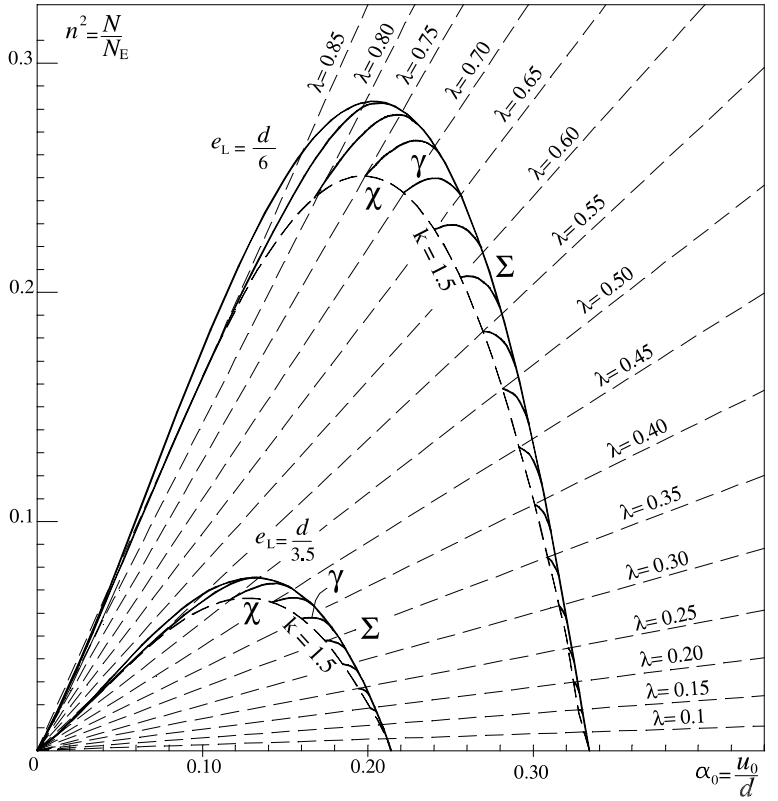

Fig. 13. Response curves of load–displacement corresponding to the eccentricity values $e_L = d/6$ and $e_L = d/3.5$, for $k = \varepsilon_0/\varepsilon_u = 1.5$.

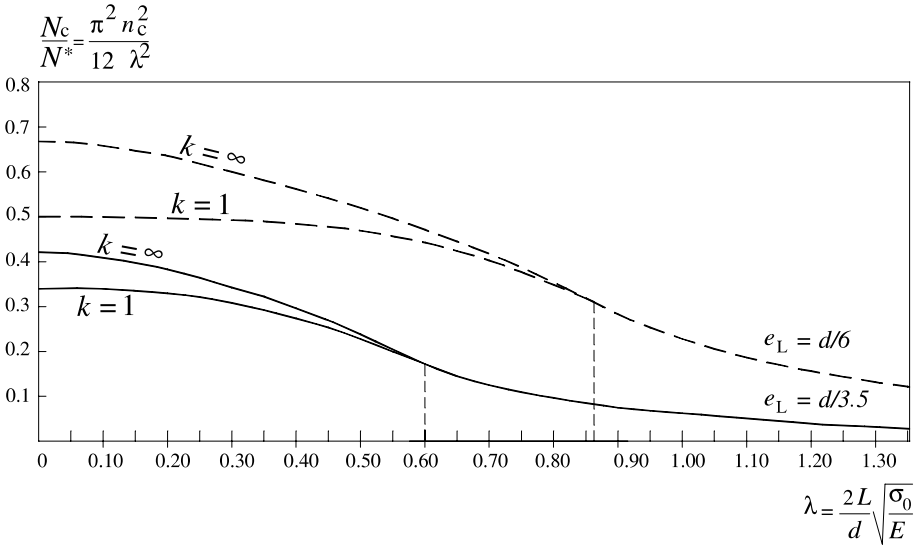

Fig. 14. Stability curves corresponding to the eccentricity values $e_L = d/6$ and $e_L = d/3.5$ for $k = 1$ and $k = \infty$.

of the middle section, and we have $N_c/N^* = 3/2\alpha_L$. These curves are analogous to those calculated by Angervo (1954) and generalised by Sahlin (1971), under the hypothesis that the material exhibits linear elastic behaviour under compression up until crushing. Instead, for $k = \infty$, failure comes about by crushing when the stress distribution in the compressed section is constant at a value of σ_0, and $N_c/N^* = 2\alpha_L$.

For increasing values of slenderness, the ratio N_c/N^* decreases, and for each value of e_L, there is a value of λ beyond which the two curves relative to $k = 1$ and $k = \infty$ coincide. Clearly, the interval between these two curves contains the situations relative to all values of $k > 1$.

Once these curves have been plotted for a large enough number of values of eccentricity e_L and parameter k, as the geometric (d, h, L) and mechanical $(E, \sigma_0 \varepsilon_u)$ characteristics of the beam are known, it is possible to calculate the critical load value as a function of λ for each value of the assumed limit strain.

4. Applications

By way of example, we shall now illustrate application of the model to the study of compressed piles. To this end, let us consider the case of a pile, constrained as in Fig. 6, whose features are typical of Italian renaissance cloisters and arcades.

Given the following parameter values:

$$2L = 5 \text{ m}, \quad b = d = 0.4 \text{ m}, \quad \sigma_0 = 6 \text{ MPa}, \quad E = 6000 \text{ MPa},$$

the corresponding slenderness value is $\lambda = 0.39$ and the critical Eulerian load is $N_E = 168.4 \times 10^4$ N.

Now, we intend to compare the limit load of the pile in the case of infinite compressive strength with that for limited compressive strength, for both infinite and limited ductility and the two values of load eccentricity, $e_L = d/6$ and $e_L = d/3.5$. For the case of infinite compressive strength, with the help of the curves in Fig. 13, we obtain

$$N_{cr} = 89.7 \times 10^4 \text{ N} \quad \text{for } e_L = d/6,$$

$$N_{cr} = 46.4 \times 10^4 \text{ N} \quad \text{for } e_L = d/3.5.$$

In the case of limited material compressive strength, from the curves in Fig. 14, for $k = \infty$ we obtain

$$N_{cr} = 18 \times 10^4 \text{N} \quad \text{for } e_L = d/6,$$

$$N_{cr} = 9.6 \times 10^4 \text{N} \quad \text{for } e_L = d/3.5,$$

and for $k = 1$,

$$N_{cr} = 15.5 \times 10^4 \text{N} \quad \text{for } e_L = d/6,$$

$$N_{cr} = 8.9 \times 10^4 \text{N} \quad \text{for } e_L = d/3.5.$$

We may observe, that at least for the two analysed cases, introduction of a limit to the material's compressive strength has a considerable effect on the critical load of the pile, more than further limiting its deformability.

In applications, in order to perform a simple check of the stability of piles subjected to eccentric axial loads, we apply the so-called "capacity reduction factor" ϕ. More precisely, we require that

$$N \leqslant \phi N^*, \tag{59}$$

where N is the load acting on the pile with an assigned eccentricity and $N^* = dh\sigma_0$.

Generally, factor ϕ is dictated by governing regulations as a function of the slenderness of the pile and the eccentricity of the load.

In our model, ϕ is precisely the ratio between the collapse load N_c and N^*; which, in light of (58), is given by relation

$$\phi = \frac{\pi^2}{12}\frac{n_c^2}{\lambda^2}. \tag{60}$$

Fig. 15 shows the values of ϕ as a function of $2L/d$, for the pile of height $2L$ shown in Fig. 6 and the two values of eccentricity, $d/6$ and $d/3.5$. The curves have been calculated using relation (60) for $k = 1$ and $k = \infty$ and setting $E = 1000\sigma_0$, as suggested by Italian regulations. In order to discount cases of limited practical interest, we have limited ourselves to considering $2L/d \leqslant 25$.

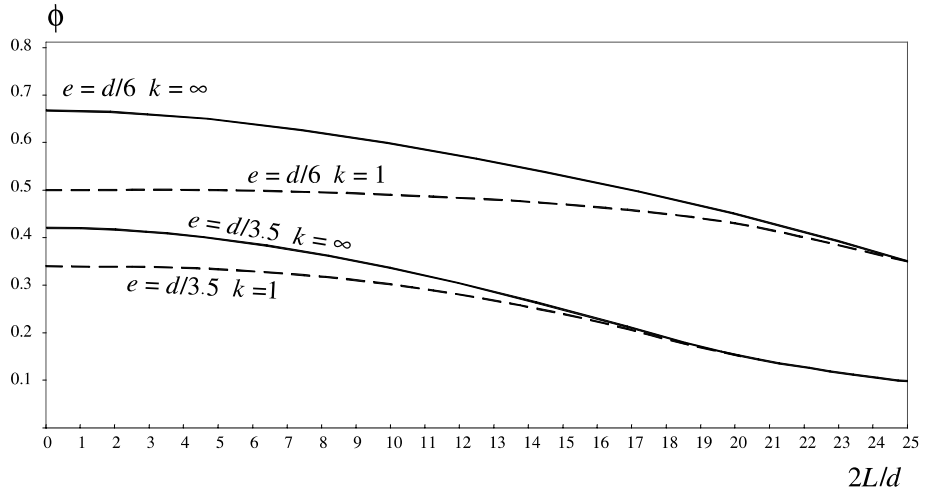

Fig. 15. Capacity reduction factor for eccentricity values $e_L = d/6$ and $e_L = d/3.5$, for $k = 1$ and $k = \infty$.

In the case of the previously analysed pile, from Fig. 15 for $k = \infty$ we obtain

$$\phi = 0.563 \quad \text{for } e_L = d/6,$$

$$\phi = 0.3 \quad \text{for } e_L = d/3.5,$$

and for $k = 1$,

$$\phi = 0.484 \quad \text{for } e_L = d/6,$$

$$\phi = 0.278 \quad \text{for } e_L = d/3.5.$$

5. Conclusions

A number of conclusions can be drawn by examining the curves in Fig. 13. Firstly, the critical load value of a non-tension-resistant material depends heavily on the load eccentricity, even if the resistance to compression is considered to be infinite (Σ curves). Moreover, by introducing a limit to the compressive strength, the resulting value of the critical load for instability failure is considerably lowered (γ curves). Finally, any further limitation on the strain makes a different (conventional) collapse mechanism possible, which may be triggered at load values below those determining instability.

The results obtained are summarised in the stability curves in Fig. 14. These allow the collapse load value to be easily deduced for each value of the hypothesised maximum admissible strain. They reveal the advantage of the material's having a certain degree of ductility under compression. It is worth noting that, for small values of λ, a considerable increase in the collapse load value results from increasing k, especially for e_L near $d/6$. In fact, as k is varied from 1 to $+\infty$, the resulting collapse load increases by about 24% for $e_L = d/3.5$ and by 33.5% for $e_L = d/6$.

Finally, by applying the model it is an easy matter to obtain curves like those shown in Fig. 15, from which the capacity reduction factor, immediately useful in applications, can be deduced.

Acknowledgements

The financial support of Progetto Finalizzato "Beni Culturali" of the Italian National Research Council (C.N.R.) and of the Progetto di Interesse Nazionale "Analisi della stabilità di strutture murarie" (COFIN 2001) are gratefully acknowledged.

References

Angervo, K., 1954. Über die Knickung und Tragfähigkeit eines excentrisch, gedrückten Pfeilers. Staatliche Technische Forschungsanstalt, pubb. 26, Helsinki.

Chapman, J.C., Slatford, J., 1957. The elastic buckling of brittle columns. Proc. Inst. Civ. Eng. 6, 107.

Frisch-Fay, R., 1975. Stability of masonry piers. Int. J. Solids Struct. 11 (2), 187–198.

Frisch-Fay, R., 1981. Quasi-analytical method for the analysis of a masonry column with a nonlinear stress–strain law. Int. J. Masonry Const. 2 (1), 41–46.

Sahlin, S., 1971. Structural Masonry. Prentice-Hall, Englewood Cliffs, NJ.

Yokel, F.Y., 1971. Stability and load capacity of members with no tensile strength. Proc. ASCE 97 ST7, 1913–1926.

Zani, N., 2001. Un'equazione costitutiva per travi costituite da materiale non resistente a trazione e con limitata resistenza a compressione. Report CNUCE B4 – 2001 006.